LOFAR Observations of Lightning Initial Breakdown Pulses

Liu, Ningyu Y.; Scholten, Olaf; Hare, Brian M.; Dwyer, Joseph R.; Sterpka, Christopher F.; Kolmašová, Ivana; Santolík, Ondřej

Published in:
Geophysical research letters

DOI:
10.1029/2022GL098073

AGU ADVANCING EARTH AND SPACE SCIENCE

Geophysical Research Letters®

RESEARCH LETTER
10.1029/2022GL098073

Key Points:

- The electrical breakdown generating lightning initial breakdown pulses has complex spatial and temporal properties
- Spatially and temporally separated VHF bursts occur during an initial breakdown pulse, coincident with brief wideband magnetic field pulses
- Generation of initial breakdown pulses likely involves multiple corona bursts, and multiple space stems/leaders and their connections

Supporting Information:

Supporting Information may be found in the online version of this article.

Correspondence to:

N. Y. Liu,
Ningyu.Liu@unh.edu

Citation:

Liu, N. Y., Scholten, O., Hare, B. M., Dwyer, J. R., Sterpka, C. F., Kolmašová, I., & Santolík, O. (2022). LOFAR observations of lightning Initial breakdown pulses. *Geophysical Research Letters*, *49*, e2022GL098073. https://doi.org/10.1029/2022GL098073

Received 26 JAN 2022
Accepted 4 MAR 2022

LOFAR Observations of Lightning Initial Breakdown Pulses

Ningyu Y. Liu[1], Olaf Scholten[2], Brian M. Hare[2], Joseph R. Dwyer[1], Christopher F. Sterpka[1], Ivana Kolmašová[3,4], and Ondřej Santolík[3,4]

[1]Department of Physics and Astronomy & Space Science Center (EOS), University of New Hampshire, Durham, NH, USA, [2]Kapteyn Astronomical Institute, University of Groningen, Groningen, The Netherlands, [3]Department of Space Physics, Institute of Atmospheric Physics of the Czech Academy of Sciences, Prague, Czechia, [4]Faculty of Mathematics and Physics, Charles University, Prague, Czechia

Abstract This paper reports an observational study of lightning initial breakdown pulses (IBPs) using the low-frequency array radio telescope and a broadband magnetic field sensor. The data show that the overall spatiotemporal evolution of the electrical breakdown causing an IBP is rather complex. During an IBP, spatially and temporally separated bursts of very high frequency (VHF) electromagnetic radiation occur in a volume on the order of 100^3 m^3, and they are coincident with brief magnetic field pulses, indicating that the location of the active breakdown region can change suddenly. Furthermore, recurrent breakdown activity is observed, especially at the location of the VHF burst. Interpreting each VHF burst as being generated by a corona burst, an IBP pulse appears to start off from an initial corona burst and subsequent corona bursts enhance it. We further suggest that the generation of IBPs likely involves multiple space stems/leaders and connections between them.

Plain Language Summary Lightning initiation is difficult to study because it occurs deep inside thunderclouds and in-situ measurements are hard if not impossible. Strong low frequency radio pulses known as initial breakdown pulses (IBPs) are generated during the initiation stage of lightning. This study uses the LOFAR radio telescope to paint a picture of the electrical breakdown activity during IBPs. The picture shows that the breakdown activity is rather complex, involving sudden change of the active breakdown location and recurrent activity in a relatively large volume.

1. Introduction

Initial breakdown pulses (IBPs) are electromagnetic field pulses emitted by lightning during the initiation stage. They are typically recorded by a broadband radio frequency sensor covering very low frequency band through medium frequency band (e.g., 1 kHz–1 MHz). IBPs are among the largest electromagnetic field pulses produced by lightning, and their average amplitude is only 2–5 times smaller than that of lightning return strokes (Marshall et al., 2014). They have a duration of 20–100 μs, with a mean of ∼60 μs (Rakov & Uman, 2003, p. 8). They tend to form a pulse train, with two consecutive pulses separated by hundreds of microseconds. Individual IBP pulses typically have a characteristic bipolar waveform, with the initial half cycle shorter than the final half cycle, and there are usually subpulses (∼1 μs) on the initial half cycle. In addition, distinct, narrow (∼1 μs) pulses are also observed during lightning initiation, which have been referred to as narrow IBPs (to differentiate, the broader pulses are also called "classic IBPs"). In fact, narrow IBPs occur more frequently than classic IBPs, but their amplitude is much smaller (Nag et al., 2009).

Investigating the underlying physical process of IBPs can provide insight into poorly understood lightning initiation. Recent studies indicate that there are two pathways for lightning initiation. The first pathway begins with narrow bipolar events (NBEs), also known as compact intracloud discharges. Broadband very high frequency (VHF) radio interferometer observations indicate that NBEs are produced by a process termed fast breakdown that propagates at a speed of $\sim 5 \times 10^7$ m/s (Huang et al., 2021; Lyu et al., 2019; Rison et al., 2016; Shao et al., 2018; Stock et al., 2017; Tilles et al., 2019), which is thought to consist of a large system of streamers. Theoretical and modeling studies have found that a large system of streamers can indeed explain various electrical and spectral properties of NBEs (Liu & Dwyer, 2020; Liu et al., 2019, 2020). The other lightning initiation pathway begins with an "initiating event" that generates a brief (≤1 μs) burst of VHF radiation (Lyu et al., 2019; Marshall et al., 2019) without detectable lower frequency pulses, which amounts to 88% of the initiation events analyzed by Lyu et al. (2019). The initiating VHF event triggers an initial electric field change on a timescale of milliseconds

(Marshall et al., 2019). A possible process to generate a brief VHF burst with no or weak lower frequency components is a discharge consisting of streamers propagating in random directions (Liu & Dwyer, 2020).

Regardless, IBPs are observed afterward. Simultaneous radio and optical observations indicate that IBPs are directly related to the development of "initial leaders" (e.g., Marshall et al., 2013; Stolzenburg et al., 2013). According to Stolzenburg et al. (2013), the initial leader is a short channel that has an initial length of about 300 m, intermittently extends to 1,000–1,500 m, and eventually leads to formation of a negative stepped leader. As the initial leader extends in length, bursts of luminosity are produced and those bursts are coincident with IBPs (Stolzenburg et al., 2013, 2016). For initiation with multiple branches in the first few milliseconds, each branch begins with IBPs and propagates first as an initial leader, and some of them transition to negative stepped leaders after a few milliseconds (Stolzenburg et al., 2014). IBPs are coincident with strong VHF bursts (Kolmašová et al., 2018, 2019). Recent broadband VHF interferometer observations indicate that during the initial half cycle of the IBP, the VHF emission source appears to propagate at a speed exceeding 10^7 m/s (Belz et al., 2020; Tilles, 2020). It has been proposed that IBPs are generated by the same fast breakdown process as NBEs (Belz et al., 2020). Belz et al. (2020) also found that gamma ray production by lightning is directly connected to strong IBPs. They have suggested that the subpulses of IBPs are caused by spark-like transient conducting events embedded within the fast streamer system.

In this paper, we report coordinated observations of IBPs with the LOFAR radio telescope and a broadband magnetic field sensor. The data indicate that the active breakdown region of IBP spans a volume on the order of 100^3 m^3. In this volume, multiple VHF bursts are emitted from discrete locations, each of which is thought to be caused by a corona burst (i.e., burst of VHF emitting streamers). An IBP pulse appears to start off from an initial corona burst and subsequent corona bursts enhance it. We present a possible scenario for IBP generation that is characterized by stepwise propagation of a negative leader involving multiple space stems/leaders.

2. Observations

2.1. Instrument Description

LOFAR consists of thousands of antennas distributed over Europe. Currently, only the Low Band Antennas (LBA, 30–80 MHz) from the 37 Dutch stations are used for lightning observation. Detailed description of LOFAR and its particular operation mode for lightning studies can be found in (e.g., Hare et al., 2019; Scholten et al., 2021a; Scholten, Hare, Dwyer, Liu, et al., 2021; Scholten, Hare, Dwyer, Sterpka, et al., 2021). Broadband magnetic field measurements were provided by a magnetic loop antenna (Kolmašová et al., 2018) installed at a site, 0.6 km to the north and 15.1 km to the east of the LOFAR core. The antenna is sensitive to a frequency range from 5 kHz to 90 MHz, and the sampling frequency is 200 MHz. Details of the system can be found in (Scholten et al., 2021a, 2021b; Scholten, Hare, Dwyer, Liu, et al., 2021; Scholten, Hare, Dwyer, Sterpka, et al., 2021).

2.2. Results

We report the observations of the first three IBPs (referred to as IBP1-IBP3 below) of a lightning flash occurred on 24 April 2019 at 21:30 UTC. The flash was initiated at 4.5 km altitude and a distance of approximately 30 km from the LOFAR core. The initiation location is closer to the magnetic loop antenna, with a distance of about 20 km. The entire flash lasted over 500 ms and spawned many negative stepped leaders in the positive charge layer below 4.5 km altitude, as well as positive leader needles in the negative charge layer between 4.5 and 6 km altitude. The lowest altitude at which breakdown activity (negative stepped leaders) was observed by LOFAR is approximately 1 km, that is, no return strokes were detected, which is also confirmed by the magnetic field measurements. This is typical for LOFAR observed flashes, which suggests that thunderstorms in this region typically have an expansive lower positive charge region. The same lightning flash was also analyzed in previous studies (e.g., Scholten et al., 2021a, 2021b; Scholten, Hare, Dwyer, Liu, et al., 2021; Scholten, Hare, Dwyer, Sterpka, et al., 2021), which focused on, for example, flash development and VHF intense stages termed intensely radiating negative leaders.

Figure 1 shows the magnetic field waveform, the VHF power waveform, and the VHF emission sources obtained with the LOFAR impulsive imager (Hare et al., 2019; Scholten, Hare, Dwyer, Sterpka, et al., 2021) during the first 4 ms of the initiation and a shorter interval of 0.4–0.9 ms. The impulsive imager can efficiently obtain the

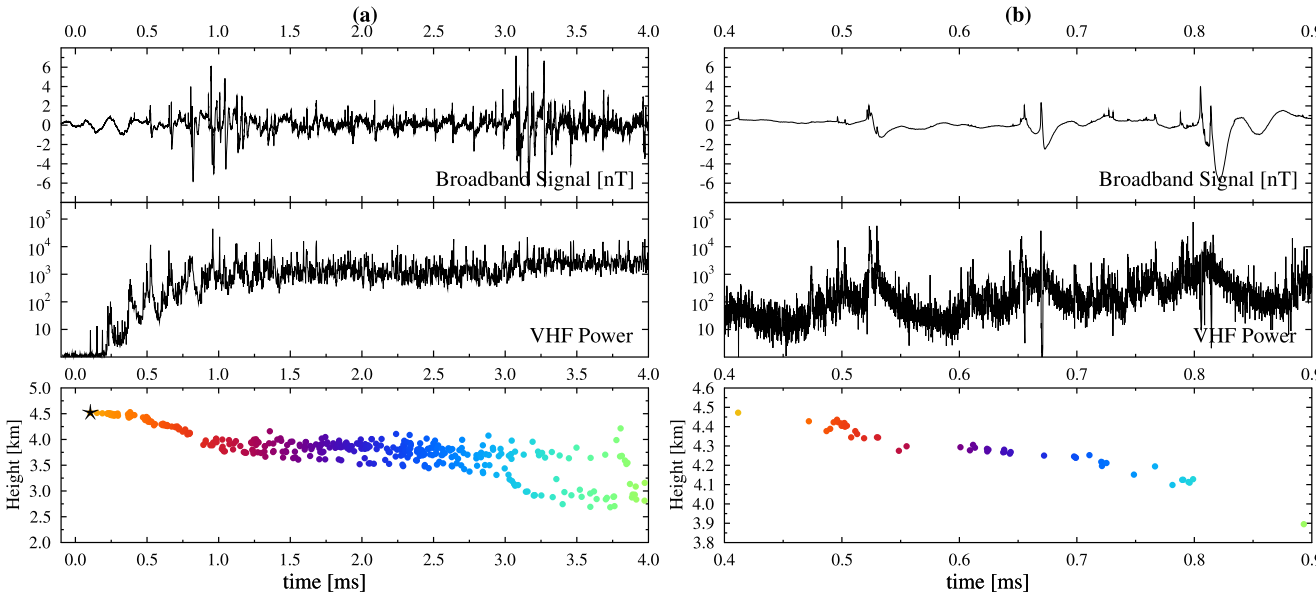

Figure 1. Overview of the initial breakdown pulses observed during the initiation of a lightning flash on 24 April 2019 at 21:30 UTC. In both (a) and (b), the three vertically arranged panels show, respectively, the magnetic loop antenna data, the VHF power from an antenna at the LOFAR core, and the VHF emission sources obtained with the LOFAR impulsive imager. The magnetic loop antenna data is averaged over 200 ns. The VHF power shown is the Hilbert envelope (the absolute value of the complex/analytic signal) of the data from the LOFAR antenna, averaged over 2 μs for (a) and 100 ns for (b) to better show the trend of the VHF power variation.

accurate locations of the sources corresponding to relatively strong and distinct LOFAR VHF pulses (approximately 100 ns wide, the width of the impulse response of the LBA antenna). At present, it is mainly used to create a map of an entire or a large portion of lightning flash for further analysis. As shown by Figure 1a, before 0.5 ms the initiating breakdown hardly moves downward. Bursts of VHF radiation start to appear at 0.1 ms. They are initially very brief and then the duration increases to tens of microseconds or longer. The initiation appears to fall into the category of lightning initiation with short VHF bursts less than 0.5 μs (Lyu et al., 2019; Marshall et al., 2019). As shown by the magnetic field waveform, IBP pulses start to appear at around 0.5 ms and increase in amplitude until 1 ms when the emission sources show development of multiple branches. From this onwards, it appears IBP pulses from different branches overlap while their amplitude decreases. The VHF power is not as bursty as the initial stage of 1.0 ms and stays at a relatively high level. Strong magnetic field pulses appear again starting at 3.0 ms, when the discharge activity can be clearly grouped into two horizontal layers. The VHF characteristics and the polarity of the magnetic field pulses indicate that the initial, downward-propagating breakdown is of negative polarity.

Using a newly developed interferometry imaging code, called time resolved interferometric 3-dimensional (TRI-D) imager, which allows for determination of a VHF emission source from the LOFAR VHF records of a 100-ns time interval (an order of magnitude smaller than the impulsive imager). Scholten, Hare, Dwyer, Liu, et al. (2021b) found that the structure of the discharge starting at 1 ms or at 3 ms is rather complex. Nearly simultaneous (within 100 μs) VHF sources are distributed in a volume of 1 km^3, with no easily discernible discharge channels. This likely indicates that simultaneous corona bursts occur in such a volume during those periods.

Figure 1b shows that the three IBPs are roughly separated by 100 μs and the pulse amplitude increases with time. The duration of an IBP pulse is about 50 μs, and there are narrow pulses superimposed on each IBP pulse. The duration and time separation between IBPs are consistent with previous observations of IBPs. There is a surge in the VHF power during each IBP, and a few emission sources are typically identified by the impulsive imager. The downward propagation direction shown by the emissions source, together with the polarity of the magnetic field pulse, indicates that the source discharge is of negative polarity.

Figure 2 shows a 50 μs interval containing IBP1 and the prior 50 μs. The LOFAR emission sources shown by the circles are obtained using the TRI-D imager, with the size of the circle proportional to the VHF power over the 100 ns time interval corresponding to that source. The discharge activity shown by the LOFAR sources provides neither an easy-to-follow picture nor any indication where the eventual lightning conducting channel

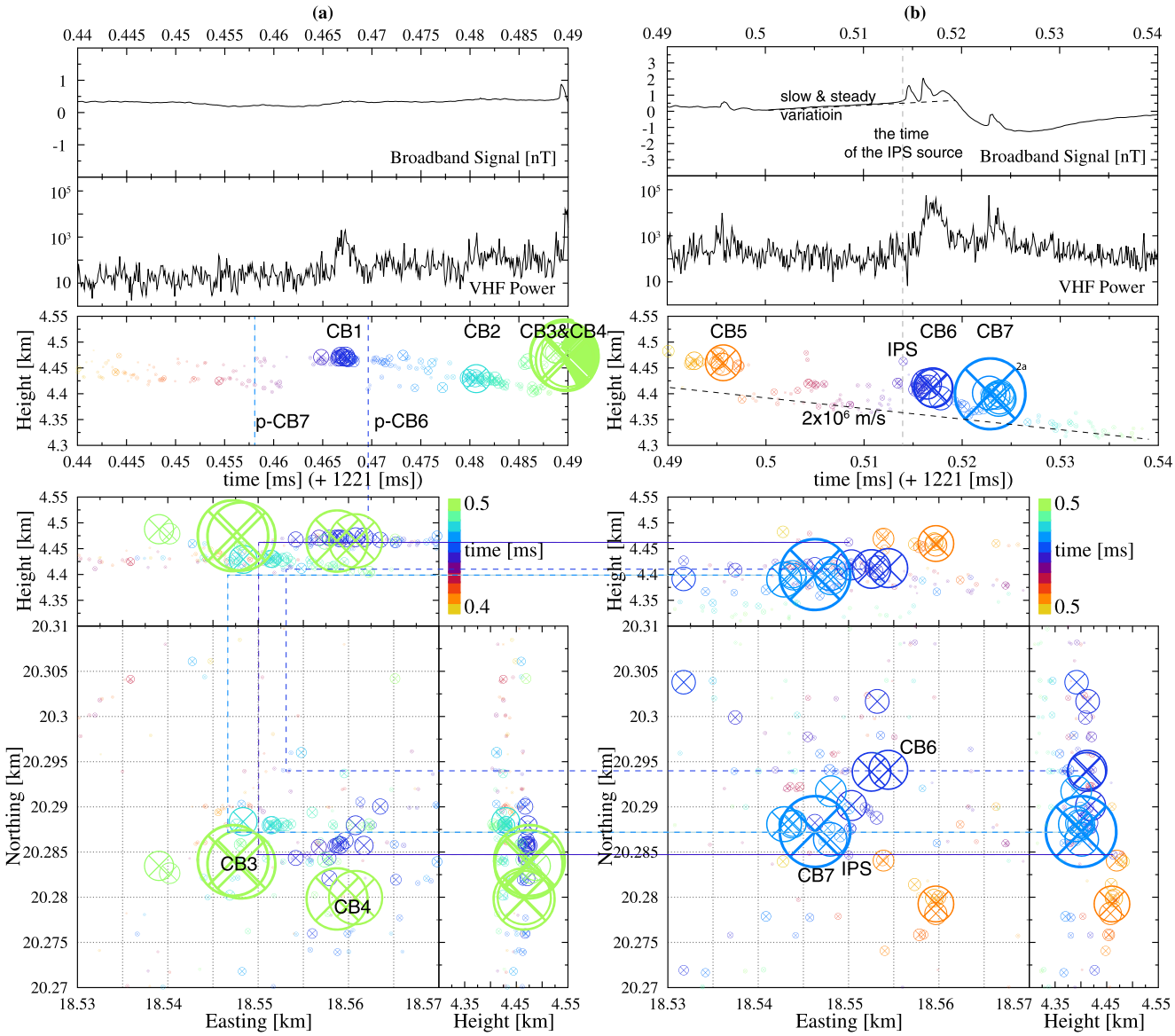

Figure 2. The first initial breakdown pulse. (a) The prior 50 μs. (b) A 50 μs time interval containing the peak of the IBP. Each column shows the magnetic loop antenna data, the VHF power from an antenna at the LOFAR core, the height versus time plot for the VHF emission sources obtained using the TRI-D imager, and the three-dimensional locations of the sources. The size of the circle representing each source is proportional to the VHF power and the center of the cross of each circle shows the location. The dashed lines in the bottom panels identify the locations of IPS, CB6, and CB7 in (a). They show that the IPS source occurs at the location of CB3 and there are prior activities at the locations of CB6 and CB7. The two vertical lines in the height versus time plot of (a) show the times of prior activities for CB6 and CB7, respectively.

is, even though IBP1 is in fact the simplest case among the three IBPs. A feature that can be readily identified is that there are a few discrete bursts of strong sources. The entire LOFAR sources are distributed in a volume of $40 \times 40 \times 175$ m^3 between 4.3 and 4.475 km altitudes, but strong sources during the IBP are located in a relatively compact horizontal area of 15×15 m^2, while spanning altitude range of 4.39–4.475 km, that is, a change of 85 m. The height versus time plots show the LOFAR source altitudes generally trend lower but weak sources at a specific time may spread over a vertical range of 50 m or so. The vertical spread in the source altitude is smaller for a period containing strong sources, but it may be because the TRI-D imager obtains only one source for a given time window, masking weak sources. In addition, although the altitudes of the bursts of strong sources decrease with time overall, a burst of strong sources at higher altitudes may follow one at lower altitudes. After each burst, there may be a sudden downward shift in the source altitude.

Consistently, the VHF power waveform shows there are intermittent VHF bursts embedded in an elevated VHF background activity. In fact, the VHF power does not stay at relatively constant level during the IBP or even just its initial cycle. It seems that brief (∼1 μs) magnetic field pulses even with small amplitude may correspond to bursts of VHF activity.

Each of those strong VHF bursts is thought to be caused by a corona burst or a burst of VHF emitting streamers and will be referred to as such below. There are at least seven corona bursts in this figure, labeled as CB1-CB7. It should be pointed out that the LOFAR emission sources tend to have a larger spread along the radial direction even if an event is observed by the LOFAR antenna from all directions (Scholten et al., 2021b). This is because that the density of the antennas decreases radially away from the LOFAR core which is at the origin on the bottom panels of Figure 2.

The IBP pulse appears to begin around 0.5 ms, as shown by the gradual but steady variation in the magnetic field waveform, which is well approximated by a linear variation as shown by the dashed line. That is preceded by three corona bursts CB3-CB5 within 10 μs (immediately preceded by CB5), which are associated with brief, bipolar magnetic field pulses. Bursts CB3 and CB4 occur nearly simultaneously (within 0.2 μs) at ≃4.475 km altitude, and they are within 10–15 m from each other for both vertical and horizontal directions. It is unclear if they are connected physically and if they are by some discharge wave, the speed of the wave is about 10^8 m/s. They are followed by CB5 5 μs later, which starts at the same location as CB4. Burst CB6 occurs 20 μs later at 4.4125 km and it is followed by CB7 at 4.4025 km after 5 μs. Interestingly, the last burst occurs right below CB2 and CB3 (see the dashed lines in the plots), with vertical separations of 30 and 70 m (note that CB2 occurs at a lower altitude than CB3), respectively. It is interesting to note that corona bursts can occur with minimal temporal (e.g., CB3 and CB4) or spatial (e.g., CB4 and CB5) separation. Not every corona burst results in discernible signatures in the magnetic field waveform, for example, CB1 and CB2, but when they do, their signatures may be represented by brief (∼1 μs), isolated bipolar pulses at 0.49 ms (CB3 and CB4) and near 0.495 ms (CB5). Finally, the black dashed line in the height versus time plot in Figure 2b shows that the leading front of the overall downward development of the discharge steadily moves downward, at a speed of approximately 2×10^6 m/s.

A few additional features can be identified upon close examination. A corona burst occurs only in a region with prior activity within 10 m or so. For example, CB5 occurs at the location of CB4; there are prior activities although weak at the locations of CB6 and CB7, as shown by the dashed lines in the bottom panels, as well as by the dashed lines that show the prior activity at the locations of CB6 and CB7 in the height versus time plot (marked by p-CB6 and p-CB7). The activity can even be 60–70 us ahead, for example, p-CB7. For at least some bursts during the IBP, they are immediately preceded by sources at higher altitudes, for example, the source labeled by immediately preceding sources (IPS) in the figure. This source occurs at the exact location of CB3, and it precedes a faster rise in the magnetic field waveform and the subsequent fall. Finally, the downward development of the discharge appears to be led by a wavefront of weak sources and corona bursts occur behind the front.

Figure 3 shows IBP2 and the time interval between IBP1 and IBP2, a total of 150 μs. The volume shown spans 100 m in either horizontal direction and 250 m in the vertical direction. Before IBP2, the discharge activity mainly extends horizontally, from the northwest to the southeast, and nearly simultaneous sources (e.g., the sources in either yellow, orange, or red color) are distributed in almost the entire horizontal region. There are bursts of enhanced VHF activity but no significant pulses in the magnetic field data. One particularly interesting source is the one at a relatively high altitude (≃4.425 km) occurring around 0.5675 ms, which is at the same location as CB6 of IBP1.

Strong VHF bursts occur during IBP2 also. In fact, two of them are so strong that they triggered a lightning protection system to shut down the antenna operation at many LOFAR stations during brief intervals around the peaks of these two bursts. The antennas, however, were fully operational for the rest periods of the two IBPs. The dips in the VHF power around 0.648 and 0.663 ms result from the activation of the lightning protection system, each coincident with a narrow pulse in the magnetic field waveform. The two pairs of vertical dashed lines in the figure roughly bound the corresponding time intervals. Considering that the VHF power is already decreased before the first VHF power dip, there is likely a separate corona burst right after the one in red in Figure 3b. So a total of five strong bursts may be identified in Figure 3b and are labeled as CB1-CB5, where CB4 and CB5 are considered as distinct bursts because of their vertical separation. The IBP pulse appears to begin with CB1, which occurs at a similar altitude as sources in Figure 3a and appears to trigger a steady increase in the magnetic field

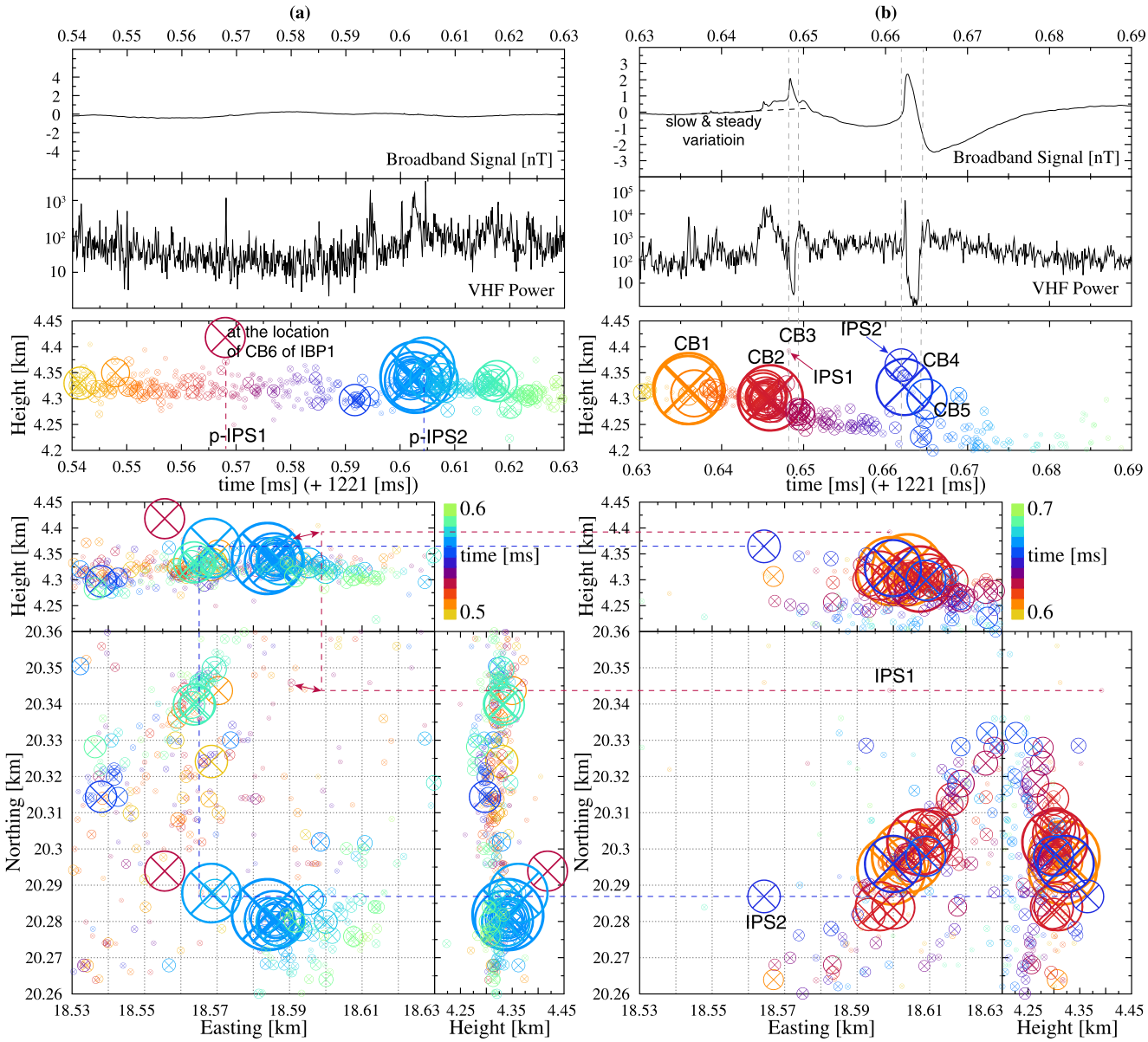

Figure 3. The second initial breakdown pulse. (a) The time interval (90 μs) between initial breakdown pulse (IBP)1 and IBP2. (b) A 60 μs time interval containing the peak of the IBP. The format of this figure is the same as Figure 2. The two pairs of the vertical dashes lines across the top three panels in (b) roughly bound the VHF power dips caused by the activation of the lightning protection system. The dashed lines across the bottom panels of both (a) and (b) identify the locations of IPS1 and IPS2 in (a). The double headed arrows in the bottom panel of (a) denote the prior source closest to IPS1.

waveform. Bursts CB2 and CB3 occur approximately 10 μs later, with coincident narrow pulses and resulting in faster rise in the magnetic field waveform. A long fall in the magnetic field waveform follows, and about 10 μs later, bursts CB4 and CB5 occur, with a simultaneous strong narrow magnetic field pulse followed by a long recovery.

The features noted for IBP1 are also found in IBP2. The strong bursts during the IBP are located in a relatively compact horizontal region and their discrete nature implies their altitude changes suddenly. The total change in the altitude of the corona bursts is on the order of 100 m. Weak sources appear to descend continuously or form a smooth descending trajectory, and strong bursts occur behind the descending wavefront formed by the weak sources. There are prior discharge activities in the locations of strong bursts. Some corona bursts are immediately preceded by sources at higher altitudes, for example, CB3 is preceded by IPS1 and CB4 by IPS2. Those high altitude sources occur at locations with prior source activity, as shown by the colored dashed lines. The prior

activities for IPS1 and IPS2 occur about 80 and 60 μs earlier, respectively (see p-IPS1 and p-IPS2 in the height vs. time plot of Figure 3a). The corona bursts preceded by such sources are associated with strong narrow pulses and are followed by a relatively long recovery in the magnetic field waveform.

IBP3 is even more complex and the lightning protection system was also activated during multiple, brief intervals. Plots similar to those in Figures 2 and 3 are shown in Figure S1 of Supplementary Information S1. It can still be seen that the VHF power is bursty and a brief magnetic field pulse (even with small magnitude) is typically associated with a VHF burst. In addition, the main IBP pulse is immediately preceded by VHF sources at higher altitudes.

Finally, it should be pointed out that although associated with the initiation of downward negative polarity breakdown, the waveforms of the three IBP pulses presented here do not look like typical classical IBPs from the initiation stage of negative cloud-to-ground lightning, but appear to be similar to those from the initiation of intracloud lightning (e.g., Weidman & Krider, 1979).

3. Discussion

Several main features in the LOFAR observations of IBPs discussed in the last section were also identified in previous observations made using interferometers with a similar bandwidth but fewer elements and shorter baselines (Belz et al., 2020; Tilles, 2020). These include: 1. IBPs are associated with strong VHF bursts; 2. The change of source altitudes during an IBP is on the order of 100 m; 3. For downward developing discharges, higher altitude sources precede the fast rise in the VHF intensity and the IBP pulse, or, lower altitude sources for upward developing discharges; and 4. Between IBPs, sources move relatively slowly. The high resolution LOFAR observations further reveal the details of the underlying process of IBPs. Most importantly, multiple corona bursts embedded in discharge activity spanning a volume of $\sim 100^3$ m^3 occur at discrete locations, and the narrow electromagnetic field pulses are coincident with the corona bursts. Furthermore, an IBP begins with a corona burst, which triggers a relatively slow variation in the magnetic field waveform, and the subsequent bursts not only generate subpulses but also enhance the IBP pulse, typically causing it to quickly reach its peak that is followed by a relatively long recovery. In addition, corona bursts occur at the locations with prior activity and the offsite sources preceding the fast VHF intensity rise also occur at locations with prior activity. The VHF picture of an IBP complements the optical picture of short, intermittently extending channel (Stolzenburg et al., 2013, 2016). The recurrent LOFAR sources at the same location after tens of microseconds likely indicate where the conducting leader is, but the total discharge volume shown from the VHF activity is rather large, instead of a thin, compact volume that may be inferred from optical observations.

Modeling work has reproduced the relatively slow variation or lower frequency components of the measured IBP pulse, as well as the related physical parameters (e.g., Carlson et al., 2015; da Silva & Pasko, 2015; Karunarathne et al., 2014; Nag & Rakov, 2016). According to simulations using transmission line models that assume a current is injected at the base of a conducting channel, a channel length of 100–1,000 m is required in order to obtain the measured IBP (Karunarathne et al., 2014). Simulations reported by da Silva and Pasko (2015) indicate that the measured IBPs can also be explained by electromagnetic transients produced during a sudden extension of a conducting leader, for example, from 700 to 1,200 m length, effectively providing an explanation for the origin of the injected current of the transmission line model. The study of Carlson et al. (2015) using three-dimensional model of lightning leader development supports that IBPs can be explained by stepwise extension of lightning leaders.

Taken together, it is reasonable to assume that a conducting leader is present prior to an IBP and in order to generate the strong amplitude of IBP pulse the leader must suddenly increase its length by hundreds of meters. In addition, there should also be processes that generate the subpulses of IBPs, which are simultaneous with VHF bursts. According to laboratory experiments of long negative discharges, the stepwise propagation of negative leaders involve multiple space stems and space leaders (Ortega et al., 1994). A space leader is formed from a space stem when it connects with another space stem developing downstream. Multiple space leaders can be formed in front of the negative stepped leader, and junctions between those space leaders can cause current pulses and corona bursts (Ortega et al., 1994). High speed optical images of negative stepped leaders of lightning have confirmed the presence of multiple space stems and space leaders during their development (e.g., Biagi et al., 2010; Hill et al., 2011; Jiang et al., 2017; Petersen & Beasley, 2013; Qi et al., 2016; Tran et al., 2014). The complexity of

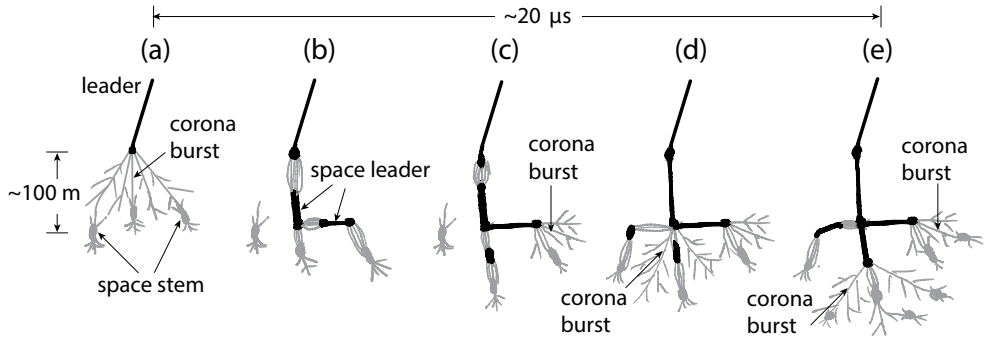

Figure 4. A diagram of the initial breakdown pulse (IBP) generation process. (a) Multiple space stems appear from the initial corona burst. (b) Two space leaders are formed, each connecting to a space stem downstream. (c) The junction of the two space leaders creates a corona burst, as well as a brief current pulse. (d) The connection between the space leader with the main leader sets off an intense corona burst. (e) Connection between a space leader further downstream with the main leader. Black and gray colors represent hot (i.e., leaders) and cold (e.g., streamers) plasma channels/structures, respectively. A corona burst is a burst of VHF emitting streamers; a space stem is a cold plasma structure that extends bidirectionally through forward propagating negative streamers and backward propagating positive streamers; and a space leader is formed when the temperature of a space stem is sufficiently high to maintain its conductivity.

the processes involved in the stepped leader propagation is also demonstrated in more recent observational and modeling studies (e.g., Ding et al., 2021; Syssoev et al., 2020).

Based on the above discussion, the IBP generation process may be represented by the diagram shown in Figure 4. The process begins with a corona burst near a leader tip, creating multiple space stems and setting off a gradually increasing current (Figure 4a). Multiple space leaders are formed, which are connected to newly formed downstream space stems, and the current continues to increase steadily (Figure 4b). Two space leaders connect with each other, generating a corona burst and a narrow current pulse (Figure 4c). In Figure 4d, the combined space leader connects with the main leader. This triggers a current surge and an intense corona burst. Afterward, the current may gradually decrease and the process reaches its end. Or as shown by Figure 4e, the main leader connects with a space leader further downstream, generating another corona burst and current pulse.

In this picture, corona bursts are triggered by the connection of conducting channels that are at different electric potentials. The connection event also leads to the narrow electromagnetic field pulse, with the required rapid current variation mostly contributed by the corona burst. The lower frequency (longer timescale) components of the IBP pulse are caused by discharge activity set up by the corona burst and redistribution of the charge after a channel connection event to equalize the channel potential. The offsite VHF sources immediately preceding the corona burst may be a manifestation of the connection event. Corona bursts without a preceding channel connection event probably also occur in nature, but it is difficult to imagine they are capable of producing significant currents by themselves if the thundercloud field is not particularly strong. That is only the corona bursts that occur as the first initiating breakdown event, such as NBEs, may create a large current required for producing electromagnetic field pulses as strong as IBPs.

Data Availability Statement

The data analyzed are available from the LOFAR Long Term Archive, under the location: "L703974_D20190424T213055.202Z_stat_R000_tbb.h5" with prefix "srm://srm.grid.sara.nl/pnfs/grid.sara.nl/data/lofar/ops/TBB/lightning/", where "stat" should be replaced by the name of the station: CS001, CS002, CS003, CS004, CS005, CS006, CS007, CS011, CS013, CS017, CS021, CS024, CS026, CS030, CS031, CS032, CS101, CS103, RS106, CS201, RS205, RS208, RS210, CS301, CS302, RS305, RS306, RS307, RS310, CS401, RS406, RS407, RS409, CS501, RS503, or RS508. To access the data, follow the instructions here: https://www.astron.nl/lofarwiki/doku.php?id=public:lta_howto, for setting up an account and "Staging Transient Buffer Board Data." Note the utility "wget" should be used as "wget https://lofar-download.grid.surfsara.nl/lofigrid/SRMFifoGet.py?surl=-location," where "location" is the location specified in above.

Acknowledgments
This research was supported in part by AFOSR Awards FA9550-18-1-0358 and FA9550-21-1-0366 to the University of New Hampshire and a subaward of DARPA HR00112120003 Grant to Embry-Riddle Aeronautical University. The work of I. Kolmašová and O. Santolík was supported by European Regional Development Fund-Project CRREAT CZ.02.1.01/0.0/0.0/15-003/0000481 and by the GACR grant 20-09671S.

References

Belz, J. W., Krehbiel, P. R., Remington, J., Stanley, M. A., Abbasi, R. U., LeVon, R., et al. (2020). Observations of the origin of downward terrestrial gamma-ray flashes. *Journal of Geophysical Research: Atmospheres*, *125*(23), e31940. https://doi.org/10.1029/2019JD031940

Biagi, C. J., Uman, M. A., Hill, J. D., Jordan, D. M., Rakov, V. A., & Dwyer, J. (2010). Observations of stepping mechanisms in a rocket-and-wire triggered lightning flash. *Journal of Geophysical Research*, *115*, 23215. https://doi.org/10.1029/2010JD014616

Carlson, B. E., Liang, C., Bitzer, P., & Christian, H. (2015). Time domain simulations of preliminary breakdown pulses in natural lightning. *Journal of Geophysical Research: Atmospheres*, *120*, 5316–5333. https://doi.org/10.1002/2014JD022765

da Silva, C. L., & Pasko, V. P. (2015). Physical mechanism of initial breakdown pulses and narrow bipolar events in lightning discharges. *Journal of Geophysical Research: Atmospheres*, *120*, 4989–5009. https://doi.org/10.1002/2015JD023209

Ding, Z., Rakov, V. A., Zhu, Y., Tran, M. D., Kostinskiy, A. Y., & Kereszy, I. (2021). Evidence and inferred mechanism of collisions of downward stepped-leader branches in negative lightning. *Geophysical Research Letters*, *48*(11), e93295. https://doi.org/10.1029/2021GL093295

Hare, B. M., Scholten, O., Dwyer, J., Trinh, T. N. G., Buitink, S., ter Veen, S., et al. (2019). Needle-like structures discovered on positively charged lightning branches. *Nature*, *568*, 360–363. https://doi.org/10.1038/s41586-019-1086-6

Hill, J. D., Uman, M. A., & Jordan, D. M. (2011). High-speed video observations of a lightning stepped leader. *Journal of Geophysical Research*, *116*. https://doi.org/10.1029/2011JD015818

Huang, A., Cummer, S. A., & Pu, Y. (2021). Lightning initiation from fast negative breakdown is led by positive polarity dominated streamers. *Geophysical Research Letters*, *48*(8), e91553. https://doi.org/10.1029/2020GL091553

Jiang, R., Qie, X., Zhang, H., Liu, M., Sun, Z., Lu, G., et al. (2017). Channel branching and zigzagging in negative cloud-to-ground lightning. *Scientific Reports*, *7*, 3457. https://doi.org/10.1038/s41598-017-03686-w

Karunarathne, S., Marshall, T. C., Stolzenburg, M., & Karunarathna, N. (2014). Modeling initial breakdown pulses of CG lightning flashes. *Journal of Geophysical Research: Atmospheres*, *119*, 9003–9019. https://doi.org/10.1002/2014JD021553

Kolmašová, I., Marshall, T., Bandara, S., Karunarathne, S., Stolzenburg, M., Karunarathne, N., & Siedlecki, R. (2019). Initial breakdown pulses accompanied by VHF pulses during negative cloud-to-ground lightning flashes. *Geophysical Research Letters*, *46*(10), 5592–5600. https://doi.org/10.1029/2019GL082488

Kolmašová, I., Santolík, O., Defer, E., Rison, W., Coquillat, S., Pedeboy, S., et al. (2018). Lightning initiation: Strong pulses of VHF radiation accompany preliminary breakdown. *Scientific Reports*, *8*, 3650. https://doi.org/10.1038/s41598-018-21972-z

Liu, N. Y., & Dwyer, J. R. (2020). Thunderstorm high frequency radio bursts with weak low frequency radiation. *Geophysical Research Letters*, *47*(23), e90325. https://doi.org/10.1029/2020GL090325

Liu, N. Y., Dwyer, J. R., & Tilles, J. N. (2020). Electromagnetic radiation spectrum of a composite system. *Physical Review Letters*, *125*(2), 025101. https://doi.org/10.1103/PhysRevLett.125.025101

Liu, N. Y., Dwyer, J. R., Tilles, J. N., Stanley, M. A., Krehbiel, P. R., Rison, W., et al. (2019). Understanding the radio spectrum of narrow bipolar events. *Journal of Geophysical Research: Atmospheres*, *124*, 10134–10153. https://doi.org/10.1029/2019JD030439

Lyu, F., Cummer, S. A., Qin, Z., & Chen, M. (2019). Lightning initiation processes imaged with very high frequency broadband interferometry. *Journal of Geophysical Research: Atmospheres*, *124*, 2994–3004. https://doi.org/10.1029/2018JD029817

Marshall, T. C., Bandara, S., Karunarathne, N., Karunarathne, S., Kolmasova, I., Siedlecki, R., & Stolzenburg, M. (2019). A study of lightning flash initiation prior to the first initial breakdown pulse. *Atmospheric Research*, *217*, 10–23. https://doi.org/10.1016/j.atmosres.2018.10.013

Marshall, T. C., Schulz, W., Karunarathna, N., Karunarathne, S., Stolzenburg, M., Vergeiner, C., & Warner, T. (2014). On the percentage of lightning flashes that begin with initial breakdown pulses. *Journal of Geophysical Research: Atmospheres*, *119*, 445–460. https://doi.org/10.1002/2013JD020854

Marshall, T. C., Stolzenburg, M., Karunarathne, S., Cummer, S., Lu, G., Betz, H.-D., et al. (2013). Initial breakdown pulses in intracloud lightning flashes and their relation to terrestrial gamma ray flashes. *Journal of Geophysical Research*, *118*, 10907–10925. https://doi.org/10.1002/jgrd.50866

Nag, A., DeCarlo, B. A., & Rakov, V. A. (2009). Analysis of microsecond- and submicrosecond-scale electric field pulses produced by cloud and ground lightning discharges. *Atmospheric Research*, *91*(2), 316–325. https://doi.org/10.1016/j.atmosres.2008.01.014

Nag, A., & Rakov, V. A. (2016). A unified engineering model of the first stroke in downward negative lightning. *Journal of Geophysical Research: Atmospheres*, *121*(5), 2188–2204. https://doi.org/10.1002/2015JD023777

Ortega, P., Domens, P., Gibert, A., Hutzler, B., & Riquel, G. (1994). Performance of a 16.7 m air rod-plane gap under a negative switching impulse. *Journal of Physics D Applied Physics*, *27*(11), 2379–2387. https://doi.org/10.1088/0022-3727/27/11/019

Petersen, D. A., & Beasley, W. H. (2013). High-speed video observations of a natural negative stepped leader and subsequent dart-stepped leader. *Journal of Geophysical Research: Atmospheres*, *118*(21), 12110–12119. https://doi.org/10.1002/2013JD019910

Qi, Q., Lu, W., Ma, Y., Chen, L., Zhang, Y., & Rakov, V. A. (2016). High-speed video observations of the fine structure of a natural negative stepped leader at close distance. *Atmospheric Research*, *178*, 260–267. https://doi.org/10.1016/j.atmosres.2016.03.027

Rakov, V. A., & Uman, M. A. (2003). *Lightning: Physics and effects*. Cambridge University Press.

Rison, W., Krehbiel, P. R., Stock, M. G., Edens, H. E., Shao, X.-M., Thomas, R. J., et al. (2016). Observations of narrow bipolar events reveal how lightning is initiated in thunderstorms. *Nature Communications*, *7*. https://doi.org/10.1038/ncomms10721

Scholten, O., Hare, B. M., Dwyer, J., Liu, N., Sterpka, C., Buitink, S., et al. (2021). Time resolved 3D interferometric imaging of a section of a negative leader with LOFAR. *Physics Review D*, *104*(6), 063022. https://doi.org/10.1103/PhysRevD.104.063022

Scholten, O., Hare, B. M., Dwyer, J., Liu, N., Sterpka, C., Kolmašová, I., et al. (2021a). A distinct negative leader propagation mode. *Scientific Reports*, *11*, 16256. https://doi.org/10.1038/s41598-021-95433-5

Scholten, O., Hare, B. M., Dwyer, J., Liu, N., Sterpka, C., Kolmašová, I., et al. (2021b). Interferometric imaging of intensely radiating negative leaders. *arXiv e-prints*. arXiv:2110.02547.

Scholten, O., Hare, B. M., Dwyer, J., Sterpka, C., Kolmašová, I., Santolík, O., et al. (2021). The initial stage of cloud lightning imaged in high resolution. *Journal of Geophysical Research: Atmospheres*, *126*(4), e33126. https://doi.org/10.1029/2020JD033126

Shao, X.-M., Ho, C., Caffrey, M., Graham, P., Haynes, B., Bowers, G., & Rassoul, H. (2018). Broadband RF interferometric mapping and polarization (BIMAP) observations of lightning discharges: Revealing new physics insights into breakdown processes. *Journal of Geophysical Research: Atmospheres*, *123*(1810), 326340–326410. https://doi.org/10.1029/2018JD029096

Stock, M. G., Krehbiel, P. R., Lapierre, J., Wu, T., Stanley, M. A., & Edens, H. E. (2017). Fast positive breakdown in lightning. *Journal of Geophysical Research: Atmospheres*, *122*, 8135–8152. https://doi.org/10.1002/2016JD025909

Stolzenburg, M., Marshall, T. C., Karunarathne, S., Karunarathna, N., & Orville, R. E. (2014). Leader observations during the initial breakdown stage of a lightning flash. *Journal of Geophysical Research: Atmospheres*, *119*(12), 221–312. https://doi.org/10.1002/2014JD021994

Stolzenburg, M., Marshall, T. C., Karunarathne, S., Karunarathna, N., Vickers, L. E., Warner, T. A., et al. (2013). Luminosity of initial breakdown in lightning. *Journal of Geophysical Research: Atmospheres*, *118*, 2918–2937. https://doi.org/10.1002/jgrd.50276

Stolzenburg, M., Marshall, T. C., Karunarathne, S., & Orville, R. E. (2016). Luminosity with intracloud-type lightning initial breakdown pulses and terrestrial gamma-ray flash candidates. *Journal of Geophysical Research: Atmospheres*, *121*(10), 936–1010. https://doi.org/10.1002/2016JD025202

Syssoev, A. A., Iudin, D. I., Bulatov, A. A., & Rakov, V. A. (2020). Numerical simulation of stepping and branching processes in negative lightning leaders. *Journal of Geophysical Research: Atmospheres*, *125*(7), e31360. https://doi.org/10.1029/2019JD031360

Tilles, J. N. (2020). *Broadband radio mapping and imaging of lightning processes*. Doctoral dissertation. University of New Hampshire. Retrieved from https://scholars.unh.edu/dissertation/2519

Tilles, J. N., Liu, N. Y., Stanley, M. A., Krehbiel, P. R., Rison, W., Stock, M. G., et al. (2019). Fast negative breakdown in thunderstorms. *Nature Communications*, *10*. https://doi.org/10.1038/s41467-019-09621-z

Tran, M. D., Rakov, V. A., & Mallick, S. (2014). A negative cloud-to-ground flash showing a number of new and rarely observed features. *Geophysical Research Letters*, *41*(18), 6523–6529. https://doi.org/10.1002/2014GL061169

Weidman, C. D., & Krider, E. P. (1979). The radiation field wave forms produced by intracloud lightning discharge processes. *Journal of Geophysical Research*, *84*(C6), 3159–3164. https://doi.org/10.1029/JC084iC06p03159